GAS PHASE DECOMPOSITION OF T-BUTYL METHYL ETHER CATALYZED BY DIFFERENT HYDROGEN HALIDES: A DFT STUDY

Sebastián Cuesta[1,2,3]*, **Edgar Márquez**[4] & **José Mora** [1,2,*]

Recibido: 9 de abril 2022 / Aceptado: 16 de junio 2022
DOI 10.26807/ia.v10i2.237

KEYWORDS: catalysis, DFT, hydrogen halide, reaction mechanism

ABSTRACT

The gas phase decomposition of t-butyl methyl ether catalyzed by hydrogen halides is studied. Four different hydrogen halides (fluorine, chlorine, bromine, and iodine) were evaluated to determine the electronic influence of the halogen in the reaction mechanism. To describe the mechanism, the ωB97XD/LANL2DZ level of theory was used. The reactivity order found was F<Cl<Br<I. Interestingly, the activation free energy estimated for the HCl model was 133.9 kJ/mol, which is in good agreement with the experimental one (134.3 kJ/mol). Further-

1 Universidad San Francisco de Quito, Departamento de Ingeniería Química, Grupo de Química Computacional y Teórica (QCT-USFQ), Quito, Ecuador (*correspondencia: sebastian_cuesta@yahoo.com)
2 Universidad San Francisco de Quito, Departamento de Ingeniería Química, Instituto de Simulación Computacional (ISC-USFQ), Quito, Ecuador. (sebastian_cuesta@yahoo.com, *correspondencia: jrmora@usfq.edu.ec)
3 University of Manchester, Department of Chemistry, Manchester Institute of Biotechnology, Manchester, UK (sebastian_cuesta@yahoo.com)
4 Universidad del Norte, Facultad de Ciencias Exactas, Departamento de Química y Biología, Grupo de Investigaciones en Química y Biología, Barranquilla, Colombia (ebrazon@uninorte.edu.co)

more, a correlation above 0.804 was noticed when the electronegativity, the hydrogen-halide distance, and the pKa of the hydrogen halides were compared to the thermodynamic parameters (activation free energy, enthalpy, and entropy). Analyzing the mechanism in depth through the intrinsic reaction coordinate, reaction force, and reaction electronic flux plots, it was observed that though the reaction occurs in a one-step concerted way. The mechanism could be divided into two events; the first one composed by a proton transfer from the halide to the oxygen and the carbon-oxygen bond cleavage, and the second one being the rate-limiting event which includes the proton transfer from the t-butyl to the halide and the double bond formation.

INTRODUCTION

The decomposition of several organic compounds containing an oxygen atom such as alcohols and ethers can be catalyzed by hydrogen halides (Failes & Stimson, 1962; Stimson & Watson, 1966b). VR Stimson and EJ Watson studied the gas phase decomposition of t-butyl methyl ether catalyzed by hydrogen chloride (Stimson & Watson, 1966a) and in a subsequent work, authors studied the gas phase decomposition of t-butyl ethyl ether using the same hydrogen halide (Stimson & Watson, 1966b). Several studies have been performed since then, including the decomposition mechanism of *t*-butyl isopropyl ether (Daly & Steele, 1972), t-butylamine (Maccoll & Nagra, 1971), 2,2-dimethoxypropane (Stimson & Tilley, 1972), 1,l-dimethoxyethane, and acetaldehyde dimethyl acetal (Stimson, 1971). Experimental mechanistic studies suggest the decomposition of these compounds using hydrogen halides as catalyst is molecular and homogenous (Stimson & Watson, 1966a), being the basicity of the oxygen atom a key factor in the reaction rate of the mechanism. In this sense, alcohols present lower reaction rates compared to ethers (Maccoll & Nagra, 1971). By comparing different functional groups the following reactivity was found acid<ester<alcohol<ether (Stimson & Tilley, 1972).

In 2012, Mora *et al* studied the hydrogen chloride catalyzed dehydration reaction mechanism of several tertiary alcohols (Jose R. Mora et al., 2012); while, in 2015, Julio *et al* worked on elucidating the gas phase elimination kinetics of aliphatic unsaturated aldehydes catalyzed by hydrogen chloride (Julio, Mora, Maldonado, & Chuchani, 2015). Their results suggest these reactions are homogeneous and unimolecular. Tertiary alcohol dehydration occurs through a six membered transition state, where the chloride transfers a proton to the oxygen (Maccoll & Nagra, 1971). Furthermore, the thermal deamination of primary amines catalyzed by HBr also follows the same six-membered transition state (Monascal, Cartaya, Álvarez-Aular, Maldonado, & Chuchani, 2018). Therefore, the same is believed to happen in ethers thermal decomposition where an important influence of the halide is mostly noticed. At the best of our knowledge, no studies have been performed to evaluate the influence of different halides in the gas phase thermal decomposition mechanism.

In this work, we present a computational study on the gas phase decomposition of t-butyl methyl ether catalyzed by hydrogen halides. The aim of this investigation is to get insights about the reaction mechanism while analyzing the electronic effect of changing the halide in the energy barriers and reaction rates.

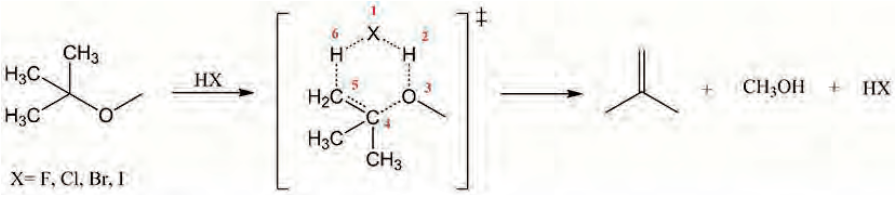

Scheme 1. T-butyl methyl ether gas phase decomposition catalyzed by hydrogen halides

COMPUTATIONAL METHODS

To characterize the gas phase decomposition of t-butyl methyl ether catalyzed by different hydrogen halides, the DFT long-range dispersion-corrected Head-Gordon hybrid functional ωB97XD (Chai & Head-Gordon, 2008b, 2008a; Grimme, 2006; Mora, Cervantes, & Marquez, 2018), as implemented in Gaussian 16 (Frisch et al., 2016) software, was used. Moreover, a LanL2DZ basis set was employed to describe the system as it has a wider application being able to correctly describe atoms from Na-La and Hf-Bi (Check et al., 2001; Farshadfar, Chipman, Yates, & Ariafard, 2019; Ganji & Ariafard, 2019; Wadt & Hay, 1985). T-butyl methyl ester, hydrogen fluoride, hydrogen chloride, hydrogen bromide, and hydrogen iodide were optimized in the gas phase. Furthermore, a frequency analysis was done at 656.15 K, which is the average temperature reported in the experiments. Berny analytical gradient optimization algorithm was employed to optimize transition state structures. Frequency calculations were later run to confirm whether the TS structure is correct by identifying only one negative frequency describing the decomposition.

To get an insight in all the changes occurring as the decomposition proceeds, the intrinsic reaction coordinate (IRC) plot was obtained (Gonzalez & Bernhard Schlegel, 1989; H. P. Hratchian & Schlegel, 2005; Hrant P. Hratchian & Schlegel, 2004). From the IRC calculation, the reaction force (RF) molecular descriptor is obtained taking the negative derivative of the energy over the normalized reaction coordinate as described in equation 1.

$$(F(\xi) = dE/d\xi) \qquad (1)$$

The RF profile is key to extract information about all the geometrical changes and electronic ones that occur as the reaction is taking place (Herrera & Toro-Labbé, 2007; Martínez & Toro-Labbé, 2009; José R. Mora et al., 2018; Toro-Labbe, 1999). In a unimolecular, concerted mechanism, the RF profile presents three zones i.e the reagents region going from the reagents (R) to ξ1; the transition state region (from ξ1 to ξ2); and the products region (from ξ2 to the

products). By integrating each zone four reaction "works" can be estimated giving information about the electronic and geometrical contributions to reach the TS and during the relaxation process in the products formation (equation 2).

$$W_x = -\int_i^j F(\xi)d\xi \qquad (2)$$

Finally, the reaction electronic flux (REF) plot was also obtained. As its name suggest, the REF describes the different electronic rearrangements happening during the reaction where positive values means spontaneous events while negative ones non-spontaneous (Duarte & Toro-Labbé, 2011; Giri, Parida, Jana, Gutiérrez-Oliva, & Toro-Labbe, 2017). Furthermore, negative values imply bond weakening while positive values bond strengthening. This descriptor is obtained using the chemical potential (μ) as described in equation 3 (Flores-Morales, Gutiérrez-Oliva, Silva, & Toro-Labbé, 2010; Herrera & Toro-Labbé, 2007).

$$J(\xi) = -d\mu/d\xi \qquad (3)$$

To obtain the chemical potential, the finite difference approximation and the theorem of Koopmans were used to be able to define in terms of the frontier molecular orbitals LUMO (Lowest Unoccupied Molecular Orbital) and HOMO (Highest Occupied Molecular Orbital) that are estimated in the gaussian calculation (equation 4).

$$\mu \cong \frac{\varepsilon_{HOMO} + \varepsilon_{LUMO}}{2} \qquad (4)$$

RESULTS

To study the gas phase decomposition mechanism of t-butyl methyl ether catalyzed by hydrogen halides (HX) and the influence of different halides in the activation mechanism, four models were built. Then, the activation free energies ($\Delta G^{\ddagger}$), activation enthalpies ($\Delta H^{\ddagger}$), and activation entropies ($\Delta S^{\ddagger}$) were obtained as shown in Table 1.

Table 1. Hydrogen-Halide bond distance (dHX), Halide electonegativity (χ), and thermodynamic parameters of the gas decomposition of t-butyl methyl ether catalyzed by hydrogen halides

Model	HX	dHX (Å)	χ	pKa	ΔG‡ (kJ/mol)	ΔH‡ (kJ/mol)	ΔS‡ (J/mol.K)
F	HF	0.94	3.98	3.1	174.8	98.9	-167.5
Cl	HCl	1.31	3.16	-6.0	133.9	68.5	-135.7
Br	HBr	1.46	2.96	-9.0	126.9	64.4	-129.0
I	HI	1.63	2.66	-9.5	123.6	67.5	-120.9

The experimental activation energies found for the gas phase decomposition of t-butyl methyl ether catalyzed by hydrogen chloride was 134.3 kJ/mol (Stimson & Watson, 1966a), which is in good agreement with the activation free energies estimated for the case of the system catalyzed with HCl (133.9 kJ/mol). Activation entropy values were all negative, which was expected as going from the reagent to the transition state implies the system becomes more organized. Results showed that as the halide position is going down in the periodic table, the activation free energy and activation enthalpy decreases, while entropy increases.

To get insights in all the changes occurring as the decomposition occurs, IRC calculations were performed on the four models (Figure 1).

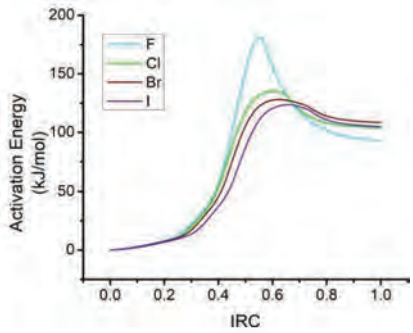

Figure 1. IRC plot of the gas decomposition of t-butyl methyl ether by hydrogen halides

The IRC profile of the studied reactions presents a similar shape, an expected result since they all describe the same reaction following the same mechanism. As the mechanism advances from the reagent to the products, the first event is a shift of the methyl group in the t-butyl making a hydrogen atom (H_2) points towards the halide. The proton is then transferred from the halide to the oxygen

while the C-O bond is cleaved. In the F model, the C-O bond is cleaved first than the H-X bond. In the Cl model, both bonds are cleaved at roughly the same time. In the Br and I models, however, the H-X bond is cleaved before the C-O. The transition state structure (Figure 2) is achieved as the second proton transfer, the one that goes from one methyl group of the t-butyl to the halide, starts. Finally, the proton is transferred to the halide and the double bond formed. The main distances for each model are shown in Table 2.

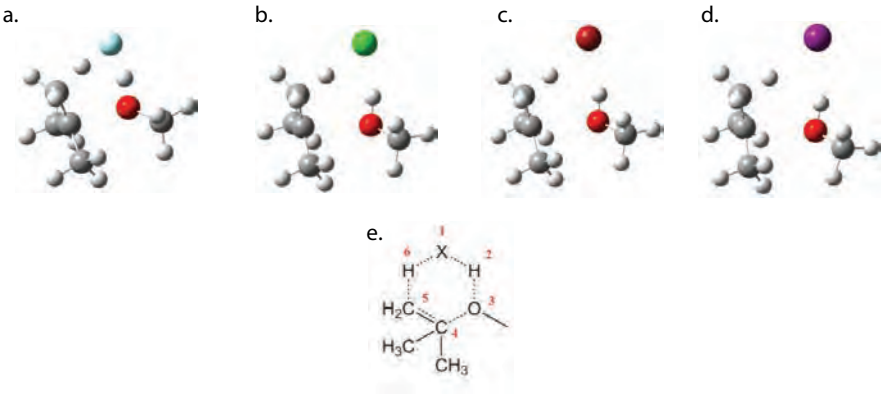

Figure 2. Transition state structures of the gas decomposition of t-butyl methyl ether catalyzed by HF (a), HCl (b), HBr (c), HI (d). e. Transition state scheme with atom labeling

Table 2. Distance of different atoms at the transition state of the gas decomposition of t-butyl methyl ether catalyzed by hydrogen halides

Model	X_1-H_2	H_2-O_3	O_3-C_4	C_4-C_5	C_5-H_6	H_6-X_1
F	1.451	1.028	2.181	1.432	1.257	1.313
Cl	2.107	0.993	2.483	1.422	1.220	1.833
Br	2.308	0.990	2.535	1.423	1.212	2.009
I	2.527	0.988	2.562	1.427	1.200	2.225

To get a better view on the geometrical and electronic changes occurring as the reaction progresses, the RF profile was plot for the four halide systems (Figure 3).

As observed in the IRC, the RF plot is also similar between the different models. Although the mechanism occurs in a concerted way, the profiles obtained present a small change in the slope around ξ=0.3. Looking at the changes occurring at this part of the mechanism, it can be seen it matches with a first event that is the proton transfer from the halide to the oxygen followed by the carbon-oxygen bond cleavage. Then, a minimum in the RF plot is observed when the second event starts i.e., the proton transfer from the t-butyl to the halide, accompanied by the double bond formation. To study the geometrical and electronic contributions, the four reaction works were estimated (Table 3) where positive work values show the system is taking up energy, and negative values means the system is giving energy (relaxation process).

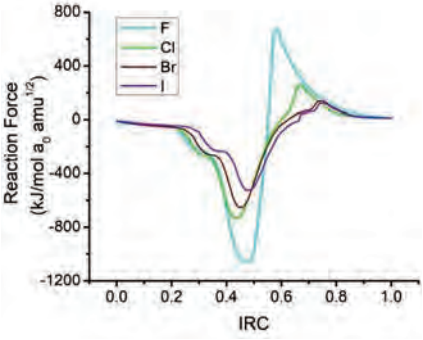

Figure 3. RF plot of the gas decomposition of t-butyl methyl ether by hydrogen halides

Table 3. Reaction works of t-butyl methyl ether catalyzed by hydrogen halides

Model	W1	W2	W3	W4
F	126.50	54.16	-11.49	-76.17
Cl	78.42	59.35	-7.94	-23.10
Br	73.71	51.22	-7.71	-12.41
I	59.00	46.05	-4.33	-11.32

To get more insights in the electronic events occurring during the gas decomposition of t-butyl methyl ether catalyzed by hydrogen halides, the REF plot was obtained (Figure 4). Same as observed in the RF plot, the main event occurs during the second proton transfer and double bond formation where a negative peak in the

electronic flux of the system can be observed. Interestingly, a positive peak is observed as H_2 is being transferred to O_3 and O_3-C_4 bond is being cleaved. After that maximum, values start going down up to the second event where any interaction between the carbon and the oxygen is lost while the C_5-H_6 weakens to start the proton transfer. Finally, all bonds start strengthening forming C=C double bond and the H-X bond.

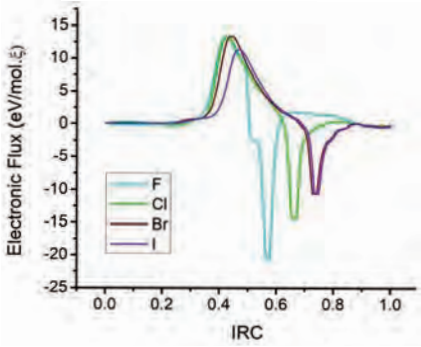

Figure 4. REF plot of the gas decomposition of t-butyl methyl ether catalyzed by hydrogen halides

DISCUSSION

The gas phase decomposition of t-butyl methyl ether catalyzed by hydrogen halides is going to produce isobutene and methanol. The results found here suggest that, as the halide is more electronegative, it requires more energy to transfer its proton to the oxygen which is detected in an increased activation energy. To get insights in this proton transfer mechanism, the electronegative values of the halides, the halide-hydrogen distance, and the pKa of the halides were related to the activation parameters estimated. A good linear correlation was achieved comparing thermodynamic parameters with the studied halides properties (R^2 values above 0.8). For the electronegativity, the highest R^2 value was obtained for $\Delta S^{\ddagger}$ (0.995) followed by $\Delta G^{\ddagger}$ (0.958), and $\Delta H^{\ddagger}$ (0.867). Furthermore, the R^2 values found for the correlation between HX distance vs thermodynamic parameters were 0.916 for $\Delta G^{\ddagger}$, 0.804 for $\Delta H^{\ddagger}$, and 0.972 for $\Delta S^{\ddagger}$. Finally, for the pKa, R^2 values of 0.991 for $\Delta G^{\ddagger}$, 0.952 for $\Delta H^{\ddagger}$, and 0.984 for $\Delta S^{\ddagger}$ were obtained. Interestingly, the highest correlation values were noticed for the correlation between thermodynamic parameters

and the halides pKa. This parameter is associated with the halogen-hydrogen dissociation energy which is key in the proton transfer event and directly influence the activation energy. High R^2 values were achieved with $\Delta S^{\ddagger}$ which is related with the loss of degrees of freedom when going from the reactant to the transition state, mainly associate with the rotation component of the partition function. $\Delta H^{\ddagger}$ present the lowest correlation values which can be attributed to the higher activation enthalpy obtained for the I model compared to the Br one.

Comparing the transition state of the different models, the distance from the halide (X_1) to the hydrogen (H_2) at the transition state increases as the electronegativity of the halide decreases ranging from 1.45 Å to 2.53 Å (Table 2). For all models, the proton of the halide is already forming a bond with the oxygen except for the F model where the bond is not fully formed. While a typical OH bond is 0.96 Å, the Cl, Br, and I models present a distance around 0.99 Å, being 0.03 Å longer for the F model. Looking at the carbon-oxygen bond cleavage (O_3-C_4), the distance is much smaller in the F model (2.18 Å) than the other three models where the distance is around 2.50 Å. Interestingly, the largest C_4-C_5 distance was found for the F model followed by the I, Br, and Cl models. This occurs because in models Cl, Br, and I, the double bond formation between C4 and C5 only depends on the H6 transfer, while in the F model apart from the proton transfer, the C4-C5 distance is influenced by O3 that is around 0.2 Å shorter than the other models. For the distance between the t-butyl carbon and the hydrogen (C_5-H_6), the distances do not vary much between the different models being around 1.20 Å. Finally, for the H_6-X_1 distance, an increase in 0.20 Å was estimated from Cl to Br and to I increasing to 0.50 Å when going from F to Cl.

During the mechanism, in order to achieve the transition state structure, an electronic energy of 54.16 kJ/mol, 59.35 kJ/mol, 51.22 kJ/mol and 46.05 kJ/mol is needed for the F, Cl, Br, and I models respectively. From that energy, around 60% is due to the geometrical rearrangement in all models except the F one, where geometrical contribution is 10% higher (70%).

Electronic rearrangements are between 30.0% in the F model, up to 43.8% in the I model; Br model present an electronic contribution of 41.0% and the Cl one 43.1%. Once the TS is achieved, the system relaxes up to the products, where geometrical contributions are higher than electronic ones.

In the REF graph, the peak formed in the second event is greater, meaning the second proton transfer is the most energetic event and, therefore, the rate limiting step in the reaction, in accordance with the IRC and RF plots.

CONCLUSION

Study of the gas phase decomposition of t-butyl methyl ether catalyzed by hydrogen halides at the ωB97XD/LANL2DZ level of theory shows that although the mechanism is homogeneous and unimolecular, the same can be divided into two main events. Changing the halide in the reaction influence the reactivity of the reaction being the reaction catalyzed by HI the most reactive and the less reactive the one using HF. The thermodynamic parameters were observed to have a good correlation with the electronegativity of the halide and the distance of the hydrogen-halide bond. In this sense, the best correlations found were between $\Delta S^{\ddagger}$ and X, and between $\Delta S^{\ddagger}$ and H-X (0.995 and 0.972 respectively). The IRC plot shows a concerted mechanism. Looking at the RF plot, a small stabilization of the system is noticeable that matches the first proton transfer. From the estimated reaction works, it can be concluded that geometrical contribution accounts between 57% to 70% of the energy needed to reach the transition state structure, while geometrical contributions only for about 35%. Finally, the REF profile agrees with all the above mentioned where an electronic redistribution is observed during the two main events that describe this gas phase decomposition reaction.

LIST OF REFERENCES

Chai, J. Da, & Head-Gordon, M. (2008a). Long-range corrected hybrid density functionals with damped atom-atom dispersion corrections. *Physical Chemistry Chemical Physics*, *10*(44), 6615–6620. https://doi.org/10.1039/b810189b

Chai, J. Da, & Head-Gordon, M. (2008b). Systematic optimization of long-range corrected hybrid density functionals. *Journal of Chemical Physics*, *128*(8), 084106. https://doi.org/10.1063/1.2834918

Check, C. E., Faust, T. O., Bailey, J. M., Wright, B. J., Gilbert, T. M., & Sunderlin, L. S. (2001). Addition of polarization and diffuse functions to the LANL2DZ basis set for P-block elements. *Journal of Physical Chemistry A*, *105*(34), 8111–8116. https://doi.org/10.1021/jp011945l

Daly, N. J., & Steele, L. P. (1972). The hydrogen chloride catalysed decomposition of t-butyl isopropyl ether. *Australian Journal of Chemistry*, *25*(4), 785–791. https://doi.org/10.1071/CH9720785

Duarte, F., & Toro-Labbé, A. (2011). The mechanism of H2 activation by (amino)carbenes. *Journal of Physical Chemistry A*, *115*(14), 3050–3059. https://doi.org/10.1021/jp1071154

Failes, R. L., & Stimson, V. R. (1962). 121. Catalysis by hydrogen halides in the gas phase. Part VI. Butan-2-ol and hydrogen bromide. *Journal of the Chemical Society (Resumed)*, *1*(1), 653–656. https://doi.org/10.1039/jr9620000653

Farshadfar, K., Chipman, A., Yates, B. F., & Ariafard, A. (2019). DFT Mechanistic Investigation into BF3-Catalyzed Alcohol Oxidation by a Hypervalent Iodine(III) Compound. *ACS Catalysis*, *9*(7), 6510–6521. https://doi.org/10.1021/acscatal.9b01599

Flores-Morales, P., Gutiérrez-Oliva, S., Silva, E., & Toro-Labbé, A. (2010). The reaction electronic flux: A new descriptor of the electronic activity taking place during a chemical reaction. Application to the characterization of the mechanism of the Schiff's base formation in the Maillard reaction. *Journal of Molecular Structure: THEOCHEM*, *943*(1–3), 121–126. https://doi.org/10.1016/j.theochem.2009.11. 013

Frisch, M. J., Trucks, G. W., Schlegel, H. B., Scuseria, G. E., Robb, M. A., Cheeseman, J. R., … Fox, D. J. (2016). Gaussian 16 Rev. B.01. Wallingford, CT.

Ganji, B., & Ariafard, A. (2019). DFT mechanistic investigation into phenol dearomatization mediated by an iodine(iii) reagent. *Organic and Biomolecular Chemistry*, *17*(14), 3521–3528. https://doi.org/10.1039/C9OB00028C

Giri, S., Parida, R., Jana, M., Gutiérrez-Oliva, S., & Toro-Labbe, A. (2017). Insights into the Mechanism of Ground and Excited State Double Proton Transfer Reaction in Formic Acid Dimer. *Journal of Physical Chemistry A*, *121*(49), 9531–9543. https://doi.org/10.1021/acs.jpca.7b09819

Gonzalez, C., & Bernhard Schlegel, H. (1989). An improved algorithm for reaction path following. *The Journal of Chemical Physics*, *90*, 2154–2161. https://doi.org/10.1063/1.456010

Grimme, S. (2006). Semiempirical GGA-type density functional constructed with a long-range dispersion correction. *Journal of Computational Chemistry*, *27*(15), 1787–1799. https://doi.org/10.1002/jcc.20495

Herrera, B., & Toro-Labbé, A. (2007). The role of reaction force and chemical potential in characterizing the mechanism of double proton transfer in the adenine-uracil complex. *Journal of Physical Chemistry A*, *111*(26), 5921–5926. https://doi.org/10.1021/jp065951z

Hratchian, H. P., & Schlegel, H. B. (2005). Using Hessian updating to increase the efficiency of a Hessian based predictor-corrector reaction path following method. *Journal of Chemical Theory and Computation*, *1*(1), 61–69. https://doi.org/10.1021/ct0499783

Hratchian, Hrant P., & Schlegel, H. B. (2004). Accurate reaction paths using a Hessian based predictor-corrector integrator. *Journal of Chemical Physics*, *120*(21), 9918–9924. https://doi.org/10.1063/1.1724823

Julio, L. L., Mora, J. R., Maldonado, A., & Chuchani, G. (2015). Gas-phase elimination kinetics of selected aliphatic α,β-unsaturated aldehydes catalyzed by hydrogen chloride. *Journal of Physical Organic Chemistry*, *28*(4), 261–265. https://doi.org/10.1002/poc.3404

Maccoll, A., & Nagra, S. S. (1971). Catalysis by hydrogen halides in the gas phase. Part XXI. Butylamine and hydrogen bromide. *Journal of the Chemical Society B: Physical Organic*, *1*(1), 1865–1869. https://doi.org/10.1039/j29710001865

Martínez, J., & Toro-Labbé, A. (2009). The reaction force. A scalar property to characterize reaction mechanisms. *Journal of Mathematical Chemistry*, *45*(4), 911–927. https://doi.org/10.1007/s10910-008-9478-0

Monascal, Y., Cartaya, L., Álvarez-Aular, Á., Maldonado, A., & Chuchani, G. (2018). The ion pair mechanism in the thermal deamination of primary amines catalyzed by HBr in the gas phase: DFT and AIM analysis. *Chemical Physics Letters*, *703*, 117–123. https://doi.org/10.1016/j.cplett.2018.05.015

Mora, J. R., Cervantes, C., & Marquez, E. (2018). New insight into the chloroacetanilide herbicide degradation mechanism through a nucleophilic attack of hydrogen sulfide. *International Journal of Molecular Sciences*, *19*(10), E2864. https://doi.org/10.3390/ijms19102864

Mora, J. R., Marquez, D. J., Marquez, E., Loroño, M., Cordova, T., & Chuchani, G. (2012). DFT studies of homogeneous catalysis in the gas phase: Dehydration kinetics of several tertiary alcohols with hydrogen chloride. *International Journal of Quantum Chemistry*, *112*(1), 78–88. https://doi.org/10.1002/qua.23145

Stimson, V. R. (1971). Catalysis by hydrogen halides in the gas phase:XXIII. 1, 1-dimethoxyethane and hydrogen bromide. *Australian Journal of Chemistry*, *24*(5), 961–968. https://doi.org/10.1071/CH9710961

Stimson, V. R., & Tilley, J. W. (1972). Catalysis by hydrogen halides in the gas phase: XXIV. 2, 2-dimethoxypropane and hydrogen chloride. *Australian Journal of Chemistry*, *25*(4), 793–801. https://doi.org/10.1071/CH9720793

Stimson, V. R., & Watson, E. J. (1966a). Catalysis by Hydrogen Halides in the Gas Phase. X. Tertiary Butyl Methyl Ether and Hydrogen Chloride. *Australian Journal of Chemistry*, *19*(3), 393–399. https://doi.org/10.1071/CH9660393

Stimson, V. R., & Watson, E. J. (1966b). Catalysis by Hydrogen Halides in the Gas Phase. XI. Tertiary Butyl Ethyl Ether and Hydrogen Chloride. *Australian Journal of Chemistry*, *19*(3), 401–407. https://doi.org/10.1071/CH9660401

Toro-Labbe, a. (1999). Characterization of chemical reactions from the profiles of energy, chemical potential and hardness. *Journal of Physical Chemistry A*, *103*(0), 4398–4403. https://doi.org/10.1021/jp984187g

Wadt, W. R., & Hay, P. J. (1985). Ab initio effective core potentials for molecular calculations. Potentials for main group elements Na to Bi. *The Journal of Chemical Physics*. https://doi.org/10.1063/1.448800